ORIGINAL PAPER

THE INFLUENCE OF THIN MULTI-LAYER OXIDE COATINGS MADE BY EB-PVD, ON THE CORROSION OF 316 L STAINLESS STEEL

LAURENTIU MOSINOIU[1+], ARCADII SOBETKII[1+], MIRCEA CORBAN[1], RADU ROBERT PITICESCU[1*], NICOLETA ZARNESCU IVAN[1], LAURA MADALINA CURSARU[1*]

Manuscript received: 10.01.2022; Accepted paper: 21.02.2022; Published online: 30.03.2022.

Abstract. *Corrosion is a process of destroying metals (alloys) under the chemical or electrochemical action of the environment. A valuable method to improve the corrosion resistance of metals and alloys working under extreme environments based on protecting the metal substrate with different ceramic materials has been proposed. Experiments were performed by Electron Beam – Physical Vapor Deposition (EB-PVD), for deposition of multi-thin oxide layers of the type: Al_2O_3 / ZrO_2 doped with Y_2O_3 / $La_2Zr_2O_7$ / ZrO_2 doped with Ce_2O_3, on 316L stainless steel laminated sheet substrates. The influence of multi-layer oxide coatings on the corrosion of 316L stainless steel was studied by electrochemical corrosion experiments (linear polarization) in NaCl solution of different concentrations (from 0.06M to 0.6M). To highlight the microstructural aspects on the elec-trochemically corroded samples, scanning electron microscopy (SEM) analyses were performed. The coating adhesion was evaluated by scratch test. Complex multi-layer oxide coatings improve the corrosion resistance of stainless steel in dilute NaCl electrolyte solutions (0.06M and 0.2M). In contrast, for more concentrated NaCl solutions (0.4M and 0.6M), these thin multi-layer oxide coatings are more susceptible to corrosion than simple alumina coatings which have higher po-larization resistance and lower corrosion rates.*

Keywords: *stainless steel; ceramic coatings; EB-PVD; electrochemical corrosion resistance; NaCl electrolyte.*

1. INTRODUCTION

Thermal evaporation and condensation from the vapor state represent a method of thin layers deposition in vacuum, where the particles deposited in the form of vapors are electrically neutral and have an energy of 0.1-0.3 eV (1eV = 1.60 × 10-19 joules). These particles are obtained by vacuum evaporation of the solid deposition material. Among the processes developed in recent decades that apply the method of thermal evaporation in vacuum is the electron beam produced by an electron gun, known as Electron Beam – Physical Vapor Deposition (EB-PVD) method [1]. Electron beam physical vapor deposition (EB-PVD), which is a high vacuum thermal coating technology, is a simple and relatively cheap process in which a focused high energy electron beam is directed towards melting an evaporation material inside a vacuumed chamber. The evaporating material is then condensed

[1] National R&D Institute for Nonferrous and Rare Metals, Pantelimon, Romania.
[*] *Corresponding authors*: rpiticescu@imnr.ro; mpopescu@imnr.ro.
[+]These authors have equally contributed to this work.

on the surface of a substrate or component to form the film layer [2]. The dis-tinct advantages of this approach are the high deposition purity, higher crystallinity rate of the obtained material due to the thermal process, enlarged coating area, precise film thickness (deposition rate can be controlled in the range of few nanometers to microme-ters), in-situ growth monitoring, and smoothness control [3, 4]. This thermal evaporation deposition method, which uses the thermal effect of electron beam bombardment on im-pact with the material to be evaporated, was developed to ensure the evaporation of refractory materials and to eliminate the chemical reaction between the evaporator and the material to be evaporated. Currently, due to the raw materials' crisis, this process is in-creasingly used in making anti-corrosion, anti-friction, and hard coatings.

Stainless steels are passive alloys, which due to their chemical composition tend to form a thin oxide layer that inhibits the metal dissolution in corrosive environments [5]. Physical, mechanical, and anti-corrosive properties of the alloy are highly related to its microstructure, where one or two phases (i.e., austenitic, ferritic, or both) may be formed [6].

316L austenitic steel exhibit excellent mechanical properties and reasonable corro-sion resistance in different environment but it lost their properties for long service at high temperature [7-9]. Pitting corrosion has been observed both on ship components and pipelines under high temperature, relative humidity, and UV light [10].

The use of rare earth oxides was recently reported to improve hardness and corrosion resistance of surface coatings of 316L stainless steel through grain refinement of la-ser-cladded layers as well as to enhance its corrosion resistance in harsh environments such as concentrated NaCl solutions [11]. The effect of rare earth oxides on the micro-structure and corrosion behavior of laser-cladding coating on 316L stainless steel was also investigated [12].

For improving the high temperature mechanical strength and corrosion resistance, stainless steel was coated by EB-PVD method with oxide / ceramic multi layers. The pro-cess of vacuum deposition by thermal evaporation using the EB-PVD method, allows ob-taining thin films / coatings with a structural morphology of granular-columnar type, perpendicular to the interface [13].

The aim of this paper is to study the potential of EB-PVD method to obtain mul-ti-layer oxide/ceramic coatings with enhanced corrosion and erosion resistance, and re-duced oxidation at high temperatures, to increase the lifetime of different metal parts made through rolling, forging, or casting. Thus, the deposition of the following oxide mul-tilayers: Al_2O_3 / Y_2O_3 doped ZrO_2 / $La_2Zr_2O_7$ / Ce_2O_3 doped ZrO_2, on 316L austenitic stain-less steel by the EB-PVD process was experimented. The corrosion behavior was investi-gated by linear polarization in NaCl solution of different concentrations (between 0.06 and 0.6M). The coating adhesion was evaluated by scratch test and scanning electron micros-copy was performed before and after corrosion measurements to evaluate the thickness coatings and surface microstructure.

2. MATERIALS AND METHODS

2.1. MATERIALS

316L austenitic stainless steel (C – 0.03%; Cr –18.20%; Ni – 11.22%; Mn – 1.96%; Si – 0.91%) in the form of laminated sheet (2 mm thickness) was selected as a substrate for EB-PVD coatings experiments. Commercial NiCrAlY alloy powder (Amperit 413.006, containing

22 wt.% Cr, 10% wt. Al, 1 wt.% Y and Ni balance to 100 wt %) was used to deposit the bond coating prior to ceramic layer deposition. Commercial Al_2O_3 powder (Amperit 740.002, max 99.5 wt % Al_2O_3) was further deposited on the bonding coat layer. ZrO_2 powder doped with 8% Y_2O_3, $La_2Zr_2O_7$ powder and ZrO_2 powder doped with 8% Ce_2O_3 obtained by a hydrothermal process at moderate temperatures (max. 250°C) and pressures (max. 40 atm) according to the methodology described in [13, 14] were used as high temperature coatings.

2.2. METHODS

2.2.1 Coating procedure using physical vapor deposition technique

Stainless steel substrates (50x30 mm) were degreased with organic solvents in an ultrasonic bath, and then fastened to the holder device (Fig. 1). The device was mounted inside the e-beam vacuum deposition chamber equipped with 4 electron guns of 10 kW each and four water cooled crucibles (Figs. 2-3). The crucibles were loaded with the previously mentioned materials to be evaporated and further placed in the carousel for all surfaces to be exposed to the vapor flux. Advanced vacuum (approx. 10-5 Torr) and per-manent heating of the substrates (over 400°C) must be ensured inside the EB-PVD Torr deposition installation throughout the thermal evaporation process. Samples investigated in this study are presented in Table 1.

Figure 1. Fastening holder device for substrates.

Figure 2. Electron beam evaporation system EB PVD Torr.

Figure 3. Electron gun 10 kW provided with 4 crucibles placed in a carousel.

Table 1. Types of thin multi-layer oxide coatings made by EB-PVD.

Sample name	Sample type
316L	316L austenitic stainless steel (SS) – uncoated substrate
316L _Al_2O_3	SS coated by EB-PVD with Al_2O_3
316L_Al_2O_3_OPR	SS coated by EB-PVD with Al_2O_3/Y_2O_3 doped ZrO_2 /$La_2Zr_2O_7$ /Ce_2O_3 doped ZrO_2

2.2.2 Corrosion experiments

ASTM corrosion cell provided with 3 electrodes: the working electrode - the material to be analyzed, having an exposed circular surface of 1 cm^2; counter-electrode - stainless steel 316; reference electrode - Ag / AgCl in 3M KCl solution. The reference electrode is positioned close to the sample by using a Luggin capillary. These 3 electrodes are connected to a

PGSTAT 128N Autolab potentiostat / galvanostat (Methrom) connected to a computer endowed with NOVA 2.1 software. The electrolyte solution used was NaCl of different concentrations, respectively 0.06M, 0.2M, 0.4M and 0.6M, according to ASTM G61-86 standard. The experiments took place after 60 minutes of immersion of the electrodes in the studied electrolyte solution.

Linear polarization was conducted in NaCl solutions described above and consisted of i) open circuit potential (OCP) determination; ii) Linear Sweep Voltammetry (LSV), with a staircase profile, in the potential range - 0.1V÷ + 0.1V versus open circuit potential, scan rate: 0.001 V/s, step: 0.001V; iii) corrosion rate analysis, by automatically determining the following parameters from the Tafel curve:

- corrosion potential, Ecorr (V);
- corrosion current density, jcorr (A / cm^2);
- intensity of corrosion current, icorr (A);
- corrosion rate (mm / year);
- polarization resistance, Rp (Ω).

Linear sweep voltammetry from (LSV) is one of the most used methods for characterizing electrochemical corrosion. This involves scanning the working electrode potential and measuring the current response. With the help of the LSV method, valuable information about the corrosion mechanisms, corrosion rate and susceptibility to corrosion of the studied materials in various environments can be discovered. Calculating corrosion rates requires determining corrosion currents. When the mechanisms of the corrosion reaction are known, the corrosion currents can be calculated from the slopes' analysis of the Tafel curves. To perform the Tafel analysis, it is necessary to have information about the surface area of the electrode (A), the equivalent weight (the ratio between the atomic mass of the corroding metal and the number of electrons changed in the anodic dissolution reaction, EW) and the density of the material (ρ).

Corrosion rate (CR) is calculated using the following formula [15-18]:

CR = icorr*K*EW / ρ*A, where:

icorr – the current intensity; K – a constant that defines the units for the corrosion rate; EW - the equivalent weight in grams/equivalent; ρ – density (in grams/cm^3); A – Area of the sample in cm^2.

The value of K used in the corrosion rate equation is 3272 mm/(A*cm*year) for corrosion rates expressed in mm/year.

Polarization resistance is obtained from the slopes of Tafel curves. The higher the polarization resistance (Rp), the more corrosion resistant the studied material and the lower the corrosion rate over time.

2.2.3 Coating Adhesion (scratch test)

The scratch test was performed with a Scratch Test NANOVEA device, on multi-layer oxide coatings deposited by EB-PVD, on 316L austenitic stainless-steel substrate, accord-ing to ISO 20502/2005.

2.2.4 Scanning Electron Microscopy (SEM) characterization

SEM/EDS characterization was performed in Low Vacuum mode with a Quanta 250 (FEI) scanning electron microscope, of high resolution, fully digitized, endowed with XT Microscope server software and an Energy-dispersive X-Ray spectrometer consisting of ELEMENT Silicon Drift Fixed Detector, and ELEMENT EDS Analysis Software Suite. Multi-layer oxide coatings deposited by EB-PVD process have been investigated before and after electrochemical corrosion test.

3. RESULTS AND DISCUSSION

3.1. CORROSION BEHAVIOR

The results of the electrochemical corrosion test obtained for the 2 types of coatings made by EB-PVD, on 316L substrate (316L_Al_2O_3, respectively 316L_ Al_2O_3_OPR), compared to the uncoated substrate (316L) are shown in Table 2 and Fig. 4.

Table 2. Parameters of the corrosion process in NaCl electrolyte solution at different concentrations.

Samples	Corrosion potential E_{corr} (V)	Corrosion current density j_{corr} (A/cm²)	Corrosion current intensity i_{corr} (A)	Corrosion rate, CR (mm/ year)	Polarization resistance R_p (Ω)
NaCl 0.06 M					
316L	-0.331	3.8793E-06	3.8793E-06	0.0451	6717.102
316L _Al_2O_3	-0.393	3.84202E-06	3.84202E-06	0.0446	6782.284
316L_Al_2O_3_OPR	-0.428	1.64892E-07	1.64892E-07	0.0019	158028.325
NaCl 0.2 M					
316L	-0.383	8.38648E-07	8.38648E-07	0.0097	31071.052
316L _Al_2O_3	-0.412	9.8423E-07	9.8423E-07	0.0114	26475.195
316L_Al_2O_3_OPR	-0.397	6.72103E-07	6.72103E-07	0.0078	38770.333
NaCl 0.4 M					
316L	-0.400	1.09572E-05	1.09572E-05	0.1273	2378.126
316L _Al_2O_3	-0.390	3.16502E-06	3.16502E-06	0.0368	8233.009
316L_Al_2O_3_OPR	-0.399	8.52749E-06	8.52749E-06	0.0991	3055.725
NaCl 0.6 M					
316L	-0.381	5.13608E-06	5.13608E-06	0.0597	5073.452
316L _Al_2O_3	-0.404	1.18584E-06	1.18584E-06	0.0138	21974.028
316L_Al_2O_3_OPR	-0.411	2.23252E-06	2.23252E-06	0.0259	11671.884

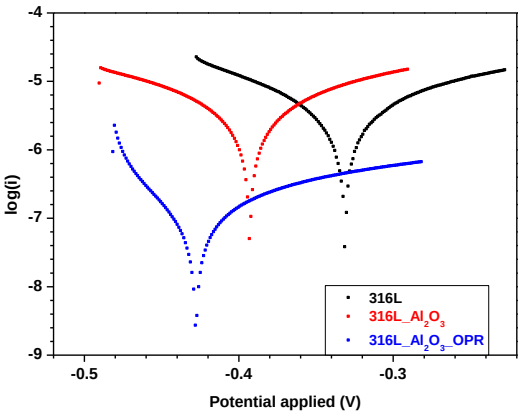

a) Tafel curve in NaCl 0.06 M

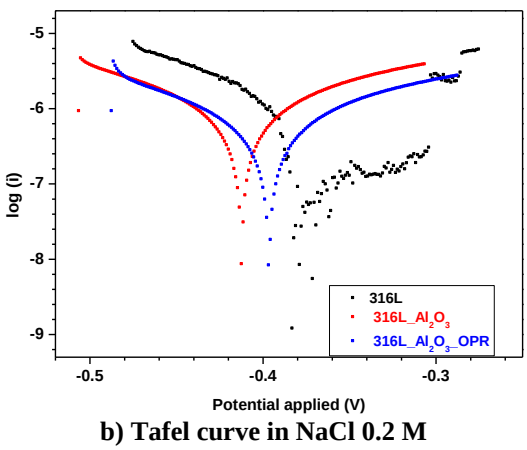

b) Tafel curve in NaCl 0.2 M

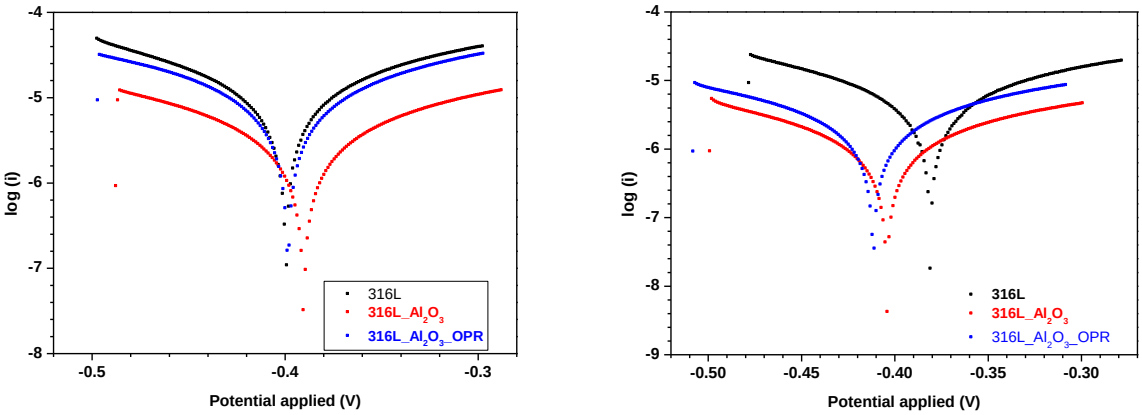

c) Tafel curve in NaCl 0.4 M **d) Tafel curve in NaCl 0.6 M**

Figure 4. Tafel curves of the studied samples in NaCl solution of different concentrations.

As it can be seen from Table 2, rare earth coatings (Al_2O_3_OPR) improve the corrosion resistance of stainless steel in dilute NaCl electrolyte solutions (0.06M and 0.2M). In contrast, for more concentrated NaCl solutions (0.4M and 0.6M), rare earth coatings (Al_2O_3_OPR) are more susceptible to corrosion than alumina coatings which have higher polarization resistance and lower corrosion rates.

3.2. SCRATCH TEST

The scratch test was performed on oxide multi-layers coatings of Al_2O_3 and OPR deposited by EB-PVD, on 316L austenitic stainless-steel substrate. In this test, a stylus was used in the form of a sharp tip (stylus) with a diameter of 50 μm that moves continuously at a speed of 0.641[mm/min] and it is pressed normally on the surface of the deposited film (Al_2O_3_OPR) on a 316L austenitic stainless-steel substrate, with a loading speed of 5 [N/min], as shown in Fig. 5a. From the scratch picture in Fig. 5b it is observed that with the increase of the normal force, the coating falls first cohesively and then adhesively.

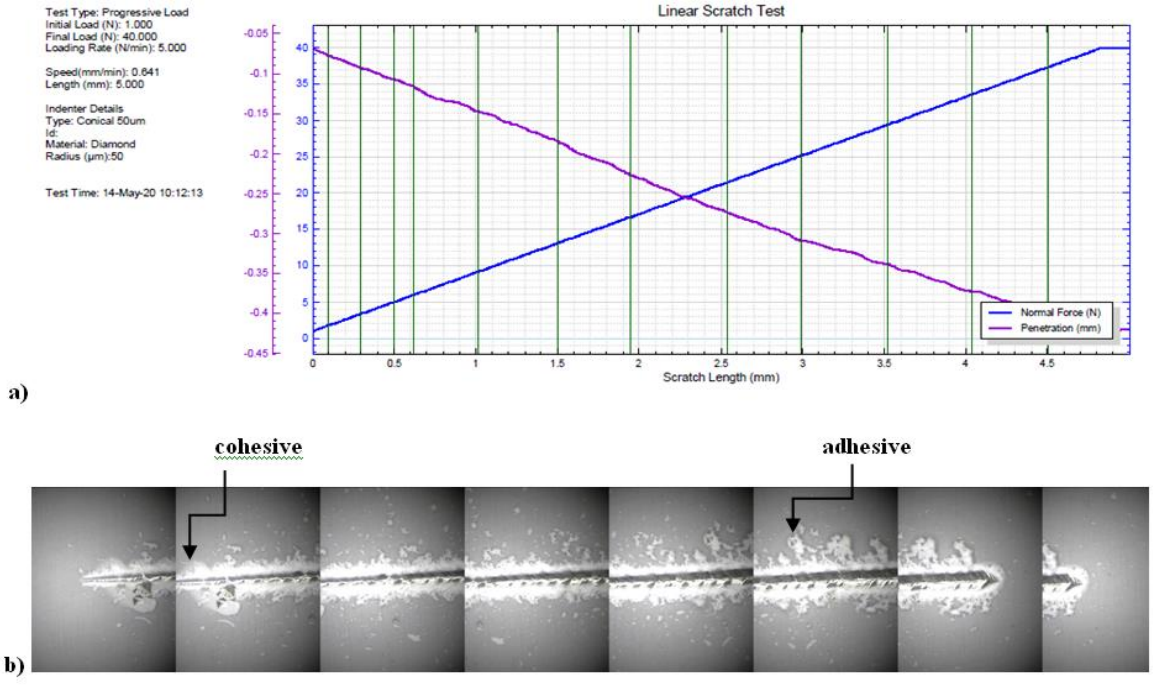

Figure 5. a) Linear scratch test and b) scratch picture of the multi-layer oxide coating scratch.

3.3. SCANNING ELECTRON MICROSCOPY (SEM) RESULTS

3.3.1 SEM characterization of the samples before corrosion experiments

Samples presented in Table 1 were studied by scanning electron microscopy in Low Vacuum mode using the secondary electron detector (LFD), the backscattered secondary electrons (CBS) and dispersive energy spectroscopy detector (EDS). The analyses were performed both on the surface of the samples (before corrosion experiments, Fig. 6) and in section (Fig. 7). In the case of surface analyses, the samples were fixed directly on the C-band, and for the analyses performed in section, the samples were embedded in epoxy resin, then sanded and polished. The microstructures of the initial, uncoated substrate (316L) and of the coatings (316L_Al_2O_3 and 316L_Al_2O_3_OPR, respectively), were studied on the surface. The roughness of the substrate (316L) and deposited layers (316L_Al_2O_3 and 316L_Al_2O_3_OPR, respectively) were studied in section. The analyzes carried out on samples surface indicate, in the case of 316L sample, a microstructure formed of polyhedral grains (Fig. 6a) and a uniform deposition, in the case of coated samples, the latter being formed, on the surface, of a granular mass with different size and structures (Figs. 6b-c).

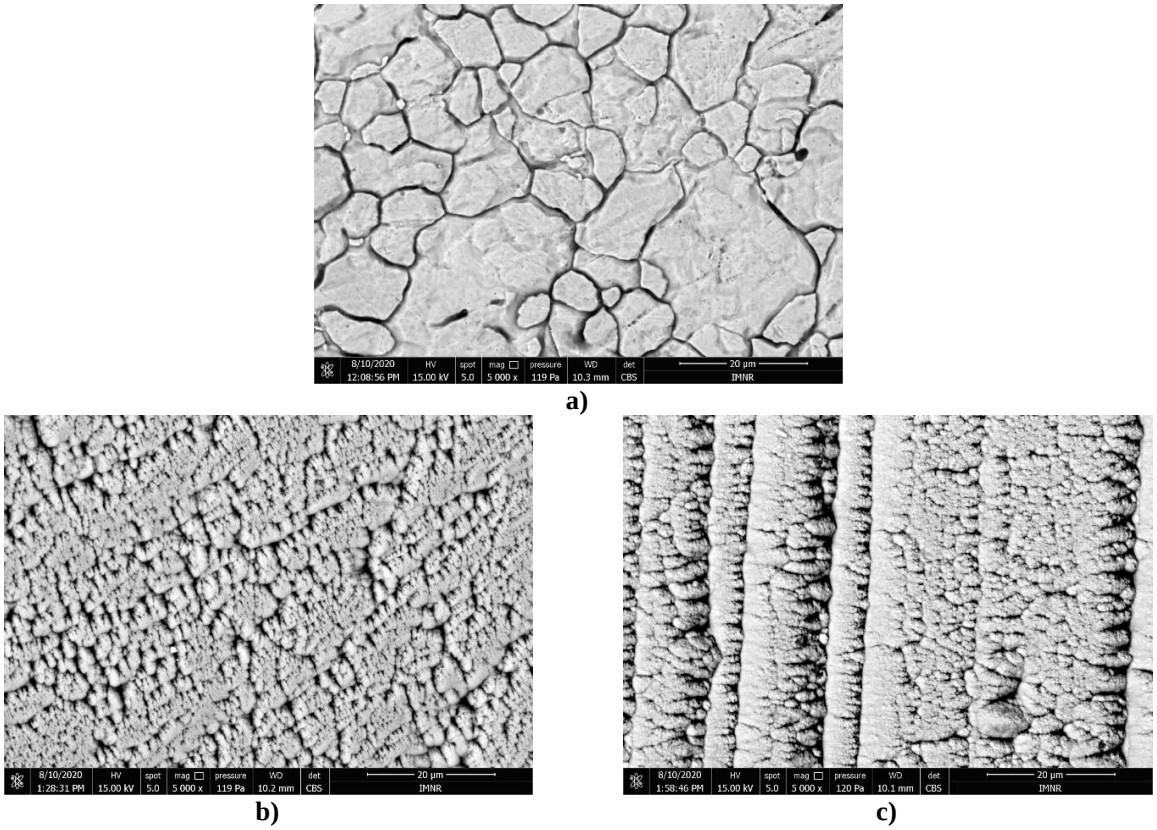

Figure 6. SEM images of samples: a) 316L; b) 316L_Al_2O_3; c) 316L_Al_2O_3_OPR.

Semi-quantitative energy dispersive spectrum (EDS) analysis performed on the surface of the samples highlighted the presence of the following elements: Fe, Cr, Ni, Mn, Si, O, C (for 316L sample); Al, O (for 316L_Al_2O_3 sample) and Zr, Ce, La, Al, O, C (for 316L_Al_2O_3_OPR sample). The results are shown in Table 3.

Table 3. EDS analysis on samples surface before corrosion experiments.

Sample	Element (line)	Weight %	Atomic %
316L	C (K)	1.67	6.90
	O (K)	2.10	6.50
	Si (K)	0.24	0.42
	Cr (K)	18.87	18.00
	Mn (K)	1.14	1.03
	Fe (K)	68.43	60.77
	Ni (K)	7.55	6.38
316L _Al_2O_3	O (K)	48.76	61.61
	Al (K)	51.24	38.39
316L_Al_2O_3_OPR	C (K)	3.37	11.43
	O (K)	22.74	57.92
	Al (K)	1.57	2.37
	Zr (L)	46.28	20.68
	La (L)	10.45	3.07
	Ce (L)	15.58	4.53

The analyses performed in section highlighted a slightly rough layer in the case of 316L sample (Fig. 7a) and the multilayer coatings (Figs. 7b-c), which have different structures and thicknesses. The approximate average thickness of the Al_2O_3 layer is 9.5 μm, and of the OPR layer is 3.5 μm (Figs. 7b-c).

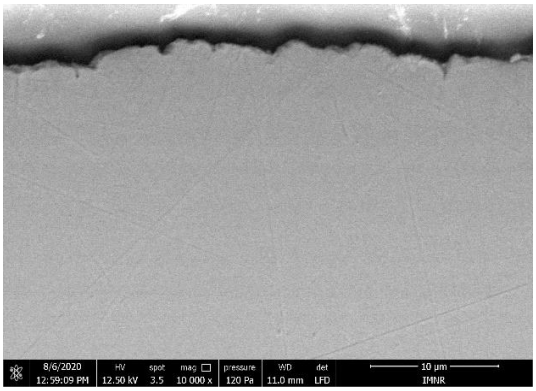

a)

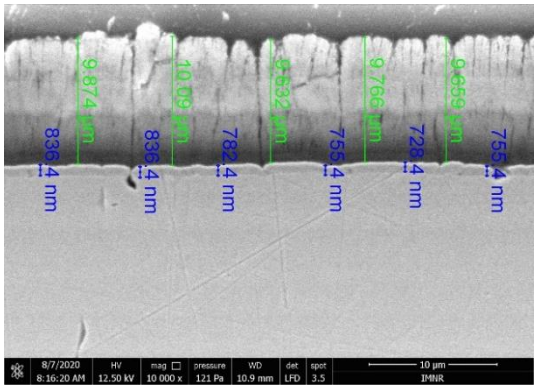

b)

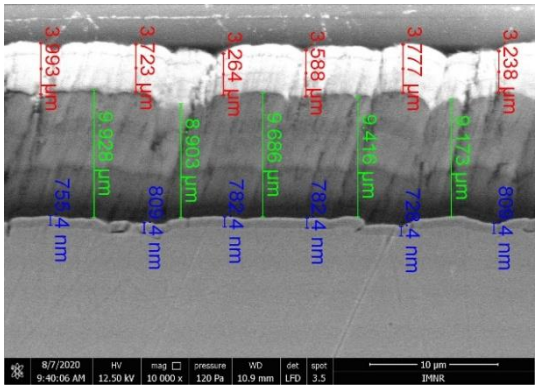

c)

Figure 7. SEM section images of samples: a) 316L; b) 316L_Al_2O_3; c) 316L_Al_2O_3_OPR.

The punctiform EDS analyzes performed in section are presented in Table 4 and highlighted the semi-quantitative chemical composition of the substrate (316L) and of each deposited layer (316L_ Al_2O_3 and 316L_ Al_2O_3_OPR), the chemical composition resulting from the analyzes being mainly composed of the elements corresponding to each constituent layer, respectively Al_2O_3 and OPR (ZrO_2-$8Y_2O_3$; $La_2Zr_2O_7$; ZrO_2-$8Ce_2O_3$), as well as the bond layer (Ni-Cr alloy) between 316Lsubstrate and ceramic layers. The presence of C in the EDS analysis is due either to the carbon strip on which the sample is fixed, or it can be explained by its presence in the embedding resin.

Table 4. EDS analysis in samples section before corrosion experiments.

Sample	Element (line)	Weight %	Atomic %
316L	C (K)	14.39	41.97
	O (K)	2.29	5.02
	Si (K)	0.22	0.28
	Cr (K)	16.70	11.25
	Mn (K)	1.00	0.64
	Fe (K)	59.30	37.20
	Ni (K)	6.10	3.64
316L _Al_2O_3	C (K)	24.81	39.31
	O (K)	30.69	36.50
	Al (K)	24.53	17.30
	Cr (K)	4.42	1.62
	Fe (K)	14.09	4.80
	Ni (K)	1.45	0.47
316L_Al_2O_3_OPR	C (K)	23.78	51.97
	O (K)	16.32	26.77
	Al (K)	3.91	3.80
	Y (L)	1.50	0.44
	Zr (L)	12.27	3.53
	La (L)	20.44	3.86
	Ce (L)	2.60	0.49
	Cr (K)	4.64	2.34
	Fe (K)	13.12	6.17
	Ni (K)	1.43	0.64

3.3.2. SEM characterization of the samples after corrosion experiments

Samples presented in Table 2 were studied by SEM after being subjected to electrochemical corrosion test in NaCl solution of different concentrations. It can be observed that 316L samples show a microstructure formed of polyhedral grains (Figs. 8a-b). 316L_Al_2O_3 samples show a relatively uniform deposition of the granular mass (Figs. 8c-d), while 316L_Al_2O_3_OPR samples show a discontinuity / interruption of granular mass deposition (Figs. 8e-f). As it can be observed from Figs. 8d, f, the results obtained from

corrosion experiments are confirmed by SEM characterization, 316L_Al_2O_3_OPR sample being more degraded than 316L_Al_2O_3 sample in NaCl solution 0.6M (concentrated electrolyte solution). 316L_Al_2O_3_OPR coatings improve corrosion resistance of 316L stainless steel substrate in dilute NaCl solution (0.06M), as shown in Figs. 8c, e.

Semi-quantitative energy dispersive spectrum (EDS) analysis performed on the surface of the samples highlighted, in addition to the Na and Cl elements present in the NaCl sediments, the presence of the following elements: Fe, Cr, Ni, Mn, Si, O, C (for 316L sample); Al, O, C (for 316L_Al_2O_3 sample) and Zr, Ce, La, Al, O, C (for 316L_Al_2O_3_ OPR sample). The results are shown in Table 5.

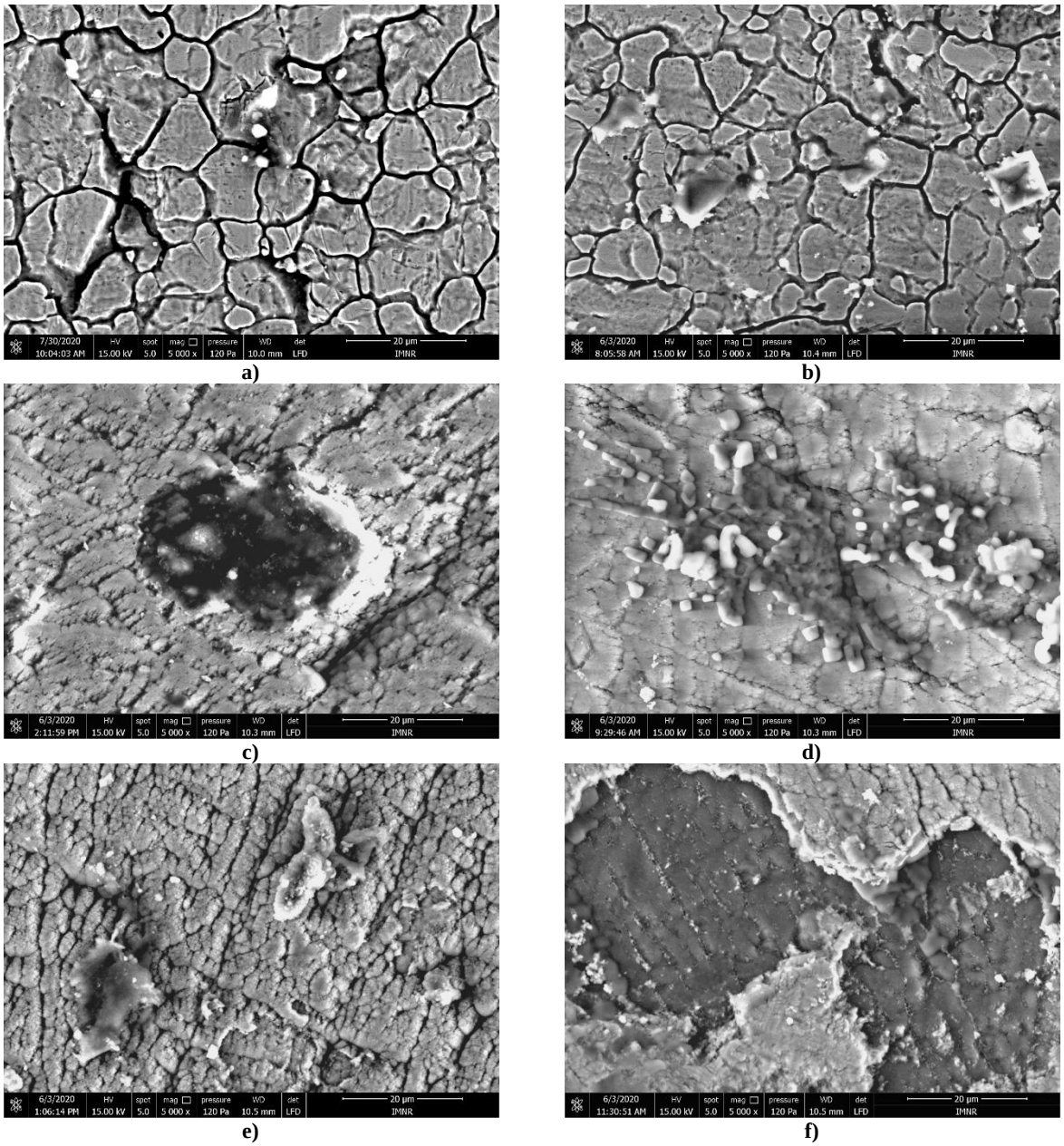

Figure 8. SEM images of the samples after corrosion experiments: a) 316L in NaCl 0.06M; b) 316L in NaCl 0.6M; c) 316L-Al_2O_3 in NaCl 0.06M; d) 316L-Al_2O_3 in NaCl 0.6M; e) 316L-Al_2O_3-OPR in NaCl 0.06M; f) 316L_Al_2O_3_OPR in NaCl 0.6M.

Table 5. EDS analysis on samples surface after corrosion experiments.

Sample	Element (line)	Weight %	Atomic %
316L	C (K)	10.70	33.66
	O (K)	2.60	6.14
	Na (K)	0.70	1.15
	Si (K)	0.26	0.35
	Cl (K)	0.16	0.17
	Cr (K)	16.60	12.06
	Mn (K)	1.01	0.69
	Fe (K)	61.51	41.62
	Ni (K)	6.46	4.16
316L _Al_2O_3	C (K)	18.36	27.33
	O (K)	40.72	45.53
	Na (K)	0.87	0.68
	Al (K)	39.47	26.17
	Cl (K)	0.57	0.29
316L_Al_2O_3_OPR	C (K)	3.08	6.62
	O (K)	38.37	61.94
	Al (K)	23.75	22.73
	Zr (L)	23.14	6.55
	La (L)	4.38	0.82
	Ce (L)	7.27	1.34

The cross-section analyses of 316L samples showed slightly rough layers and the presence of NaCl sediments in small quantities (Figs. 9a-b). In the case of 316L_Al_2O_3 samples, respectively 316L_Al_2O_3_OPR samples, cross section analyses highlighted different degradation / corrosion degrees of the deposited layers, as well as the presence of NaCl sediments. A lower degradation degree was recorded in 316L_Al_2O_3 and 316L_Al_2O_3_OPR samples immersed in NaCl 0.06M (Figs. 9c, e) while a high degree of degradation/corrosion was recorded in the case of 316L_Al_2O_3 and 316L_Al_2O_3_OPR samples immersed in NaCl 0.6M (Figs. 9d, f). The punctiform EDS analyzes performed in the samples section, presented in Table 6, highlighted the presence of the following elements: Fe, Cr, Ni, Mn, Si, O, C (for 316L sample); Al, O, Fe, Cr, Ni, C (for 316L_ Al_2O_3 sample) and Zr, Ce, La, Y, Al, O, Fe, Cr, Ni, C (for 316L_ Al_2O_3_OPR sample), in addition to the Na and Cl elements present in the NaCl sediments.

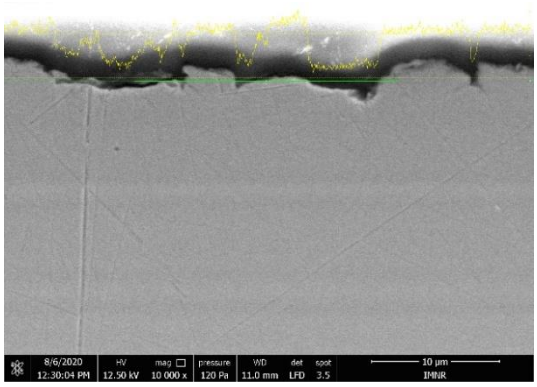

a)

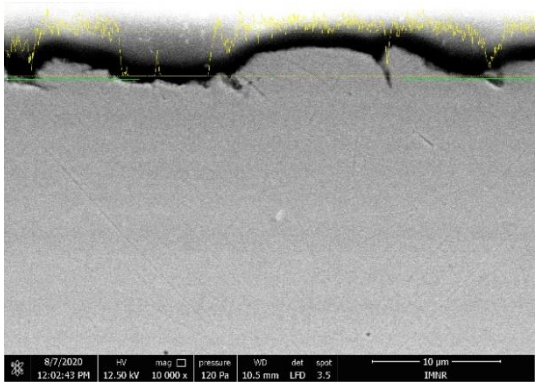

b)

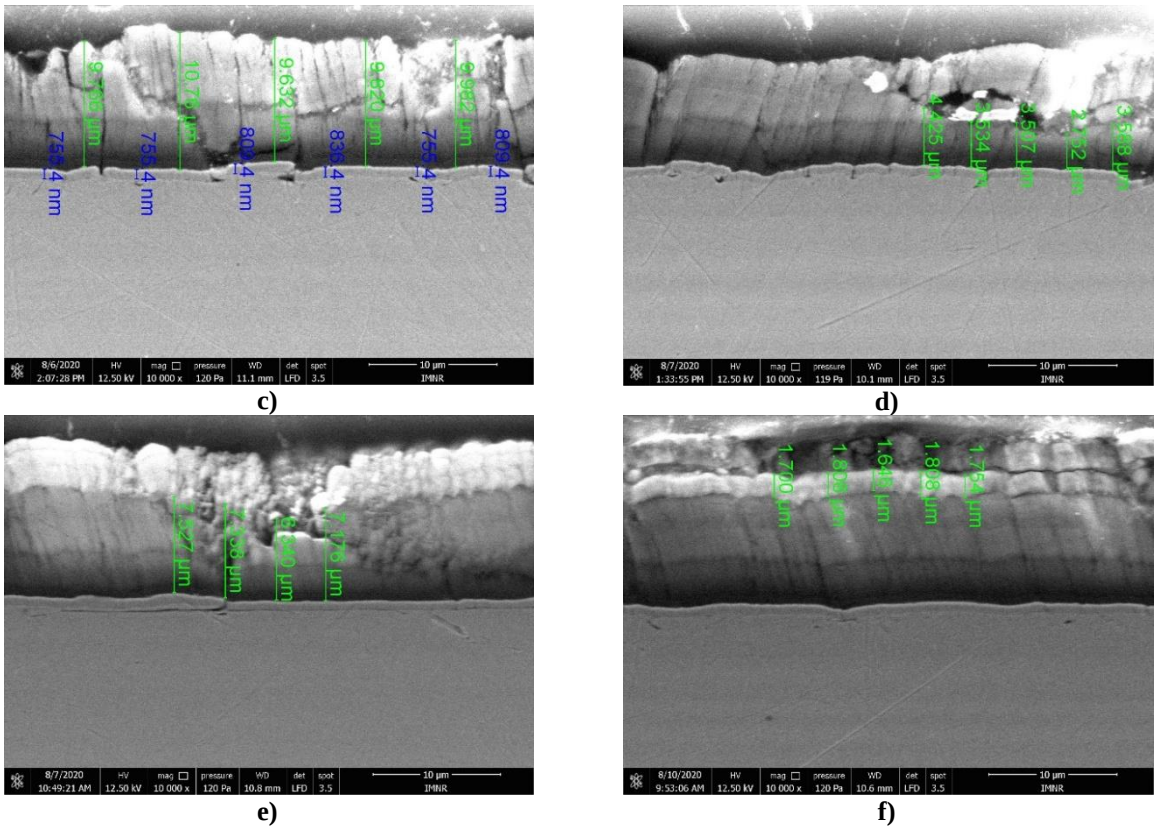

Figure 9. SEM Cross-section images of the samples after corrosion experiments: a) 316L in NaCl 0.06M; b) 316L in NaCl 0.6M; c) 316L_Al_2O_3 in NaCl 0.06M; d) 316L_Al_2O_3 in NaCl 0.6M; e) 316L_Al_2O_3_OPR in NaCl 0.06M; f) 316L_Al_2O_3_OPR in NaCl 0.6M.

Table 6. EDS analysis in samples section after corrosion experiments.

Sample	Element (line)	Weight %	Atomic %
316L	C (K)	55.21	80.21
	O (K)	6.85	7.47
	Na (K)	0.42	0.32
	Cl (K)	0.79	0.39
	Cr (K)	7.49	2.51
	Fe (K)	26.86	8.39
	Ni (K)	2.38	0.71
316L _Al_2O_3	C (K)	22.30	35.22
	O (K)	33.96	40.28
	Na (K)	0.44	0.36
	Al (K)	25.55	17.97
	Cl (K)	0.36	0.19
	Cr (K)	3.78	1.38
	Fe (K)	12.39	4.21
	Ni (K)	1.22	0.40

Sample	Element (line)	Weight %	Atomic %
316L_Al_2O_3_OPR	C (K)	26.27	54.87
	O (K)	16.21	25.41
	Al (K)	3.35	3.11
	Y (L)	0.73	0.21
	Zr (L)	14.63	4.02
	La (L)	16.78	3.03
	Ce (L)	2.47	0.44
	Cr (K)	4.58	2.21
	Fe (K)	13.38	6.01
	Ni (K)	1.59	0.68

4. CONCLUSIONS

The influence of thin oxide multilayers such as alumina and rare earth doped oxide coatings on the corrosion resistance of 316L stainless steel substrate has been studied. It has been shown that multilayer coatings such as Al_2O_3 / Y_2O_3 doped ZrO_2 / $La_2Zr_2O_7$ / Ce_2O_3 doped ZrO_2 (denoted as Al_2O_3_OPR) improve the corrosion resistance of stainless steel in diluted NaCl solutions (0.06M-0.2M). For more concentrated NaCl solutions (0.4M-0.6M), a simple alumina coating reduced by 4 times the corrosion rate of 316L stainless steel substrate. The results obtained by electrochemical corrosion experiments were confirmed by scanning electron microscopy characterization of the samples before and after corrosion tests. Further works are in course to study the corrosion mechanism and evaluate the potential use of these coatings for ship components manufactured from 316L stainless steel frequently used in marine environments.

Acknowledgement: *This research was funded by the Core Program financed by Ministry of Education and Research, grant no. PN19190401/2019-2022, "Research on obtaining multilayer oxide architectures for the substitution of critical materials used in highly corrosive environments".*

REFERENCES

[1] Ali, N., Teixeira J.A., Addali, A., Saeed, M., Al-Zubi, F., Sedaghat, A., et al., *Materials*, **12**(4), 71, 2019.
[2] Singh, J., Wolfe. D.E., *J. Mater. Sci.*, **40**(1), 1, 2005.
[3] Arunkumar, P., Aarthi, U., Sribalaji, M., Mukherjee, B., Keshri. A.K., Tanveer, W.H., et al., *J. Alloys Compd.*, **765**, 418, 2018.
[4] Moorthy, S.B.K. (Ed.), *Thin Film Structures in Energy Applications*, 1st Ed., Springer, Cham, 2015.
[5] Landoulsi, J., Genet, M.J., Richard, C., el Kirat, K., Pulvin, S., Rouxhet, P.G., *J. Colloid Interface Sci.*, **318**(2), 278, 2008.

[6] Tylek, I., Kuchta, K.,*Technical Transactions Civil Engineering / Czasopismo Techniczne Budownictwo*, **4-B**, 59, 2014.
[7] Kumar, V., Kumar, Gupta R, Das, G., *IOP Conference Series: Materials Science and Engineering*, **653**(1), 012038, 2019.
[8] Zinkle, S.J., Was, G.S., *Acta Mater.*, **61**(3), 735, 2013.
[9] Allen, T., Busby, J., Meyer, M., Petti, D., *Mater. Today*, **13**(12), 14, 2010.
[10] Jakubowski, M., *Polish Marit. Res*., **22**(3), 57, 2015.
[11] Sobetkii, A., Mosinoiu, L., Paraschiv, A., Corban, M., *Manufacturing Rev*., **7**, 33, 2020031, 2020.
[12] Xu, Z., Wang, Z., Chen, J., Qiao, Y., Zhang, J., Huang, Y., *Coatings*, **9**(10), 636, 2019.
[13] Piticescu, R.R., Corban, M., Grilli, M.L., Balima, F., Prakasam, M., *J. Nucl. Research Dev*., **18**, 18, 2019.
[14] Motoc, A.M., Valsan, S, Slobozeanu, A.E., Corban, M., Valerini, D., Prakasam, M., et al., *Metals*, **10**(6), 746, 2020.
[15] ***** *ASTM G102-89 Standard Practice for Calculation of Corrosion Rates and Related Information from Electrochemical Measurements*, 1994, available online https://idoc.pub/documents/astm-g102-standard-practice-vlr00rr05wlz, last accessed 08.01.2022.
[16] ***** *ASTM G61-86 Standard Test Method for Conducting Cyclic Potentiodynamic Polarization Measurements for Localized Corrosion Susceptibility of Iron-, Nickel-, or Cobalt-Based Alloys*, 1998.
[17] Liu, Y., Wang, Y., Lin, J., Zhou, M., Yu, F., Huang, Y., et al, *Mater. Today Commun*, **26**, 101750, 2021.
[18] Konovalova, V., *Materials Today: Proceedings*, **38**(4), 1326, 2021.